

Article

# Titanium Nanostructures: Advancing Photocatalysis in Complex Systems

Alondra A. Lugo-Ruiz <sup>1</sup> and Sonia J. Bailón-Ruiz <sup>2,\*</sup><sup>1</sup> Department of Biology, University of Puerto Rico at Ponce, Ponce, PR 00716, USA; alondra.lugo4@upr.edu<sup>2</sup> Department of Chemistry and Physics, University of Puerto Rico at Ponce, Ponce, PR 00716, USA

\* Correspondence: sonia.bailon@upr.edu; Tel.: +1-(787)-844-8181 (ext. 2338)

**Abstract:** The use of semiconductor materials, specifically TiO<sub>2</sub>, for photocatalysis of organic pollutants has gained global interest as an effective method for contaminant removal from wastewater. Titanium dioxide (TiO<sub>2</sub>) is a widely studied photocatalyst and is considered one of the best for wastewater treatments due to its high stability, affordability, and nontoxicity. The discharge of wastewater from the textile industries, which constitutes around 20% of total textile effluent, has become a significant environmental concern, posing a threat to both the aquatic ecosystem and human health. We aimed to investigate the photodegradation of organic dyes like Amaranth (AM), Methyl Orange (MO), and Quinoline Yellow (QY), individually and in combination, in an aqueous suspension with varying concentrations of TiO<sub>2</sub>. Results indicate a significant degradation of all three dyes in the multicomponent, with approximately 40% degradation in the presence of the 0.050 g/L TiO<sub>2</sub> after 360 min. These findings suggest that TiO<sub>2</sub> has a significant potential as a nanocatalyst in complex matrices.

**Keywords:** TiO<sub>2</sub>; photocatalyst; organic contaminants

## 1. Introduction

Dyes are chemically colored compounds that impart color to substrates. They have an affinity and contain both chromophore and auxochrome groups. The chromophore is the color-bearing group of the dye, determined by its saturation, while the auxochrome group controls the dye's ability to bind to the fiber. Dyes can be classified by various means, including by the source, ionic nature, application method, fiber compatibility, and constitution. Generally, they are classified by the source they are acquired from. Natural dyes, sourced from animals, plants, and minerals without any chemical treatment, are known to have minimal impact on the environment, easily biodegradability, and lack of disposable problems. However, their use often requires larger amounts and extensive dyeing process to dye a specific fabric, as opposed to synthetic dyes, and they tend to exhibit poor brightness and fastness properties, with the color tending to fade quickly. Additionally, standardization of these dyes is also difficult, due in part to the availability of the raw ingredients which may vary from location, season, and species. In contrast, synthetic dyes are highly colored organic substances that attach themselves to the fibers via chemical bonding and can be further classified based on their chemical structure or application method to the material. Notable types include azo dyes, which constitute more than 50% of synthetic dyes, contain a chromophore group, -N=N-, in their structure, and at least one nitrogen linked to an aromatic group, anionic (acid) dyes are mainly used in polyamide fibers like nylon, silk, and wool, and require an acid bath for application, and cationic (basic) dyes used in acrylic fibers, polyester, wool, and silk. Synthetic dyes have the advantage of being more readily available at a lower cost than natural dyes, they offer a wide range of colors, and provide consistent coloration across batches, unlike natural dyes that can vary in shade and quality. They also exhibit better light and wash fastness, making them



**Citation:** Lugo-Ruiz, A.A.; Bailón-Ruiz, S.J. Titanium Nanostructures: Advancing Photocatalysis in Complex Systems. *Photochem* **2024**, *4*, 222–232. <https://doi.org/10.3390/photochem4020014>

Received: 26 February 2024

Revised: 2 April 2024

Accepted: 29 April 2024

Published: 6 May 2024



**Copyright:** © 2024 by the authors. Licensee MDPI, Basel, Switzerland. This article is an open access article distributed under the terms and conditions of the Creative Commons Attribution (CC BY) license (<https://creativecommons.org/licenses/by/4.0/>).

more durable and long-lasting. Nonetheless, they are not biodegradable and are difficult to remove from textile effluents, with degradation resulting in hazardous byproducts that are released into the environment [1–8]. Based on that mentioned before, this research was focused on the photodegradation of synthetic dyes that act as contaminants (i.e., Amaranth (AM), Methyl Orange (MO), and Quinoline Yellow (QY)) by titanium-based nanomaterials. Refer to Supplementary Material (Figure S1) to view the skeletal structures of the dyes.

Amaranth is an anionic azo dye, widely used in the food and beverage industries as well as a dye for textiles such as wool and silk, leather, wood, paper coatings, and photographic industries. It can also be used as a cytoplasmic and nuclear dye in histological and hematological applications. Despite its usefulness, Amaranth is considered an endocrine disruptor and can cause irritation and redness upon contact with eyes. The United States Food and Drug Administration (FDA) withdrew its approval of the dye as a permitted coloring agent in foods and pharmaceutical products in 1976, citing positive findings in carcinogenicity tests, which were later disputed on technical grounds but have not been confirmed in subsequent tests. However, no components of Amaranth present levels greater than or equal to 0.1% as a possible or confirmed human carcinogen by the International Agency for Research Cancer (IARC) or are on the Occupational Safety and Health Administration's (OSHA) list of regulated carcinogens. The potential health risks associated with Amaranth underscore the need for further research into its use and potential impact on human health [9,10]. Methyl Orange is an anionic azo dye, with various applications in different fields. It is primarily used as a pH indicator in titration and in cell sap, as a component of a polychrome histological stain, and as a solution indicator. Additionally, it has biomedical applications, including its use in film dosimeters and as a reagent for the assay bromide. While it is not commonly used in textile applications due to its fleeting nature and sensitivity to acids, it has been used to dye wool and silk from an acid bath. In humans, oral ingestion can lead to acute toxicity [11,12]. On the other hand, Quinoline Yellow is a widely water-soluble anionic quinophthalone dye commonly employed in the food, cosmetics, and pharmaceutical industries. It also serves as a textile dye for wool, nylon, and silk. There are scarce studies about its potential genotoxic properties [13,14].

There is a significant environmental concern due to the potentially toxic and carcinogenic properties of synthetic dyes, posing a threat to living organisms and the ecosystem. The textile and dyeing industries are major contributors to water pollution, releasing a significant amount of chemical waste and dye contaminants into water bodies. According to Chandanshive et al. (2020), the annual worldwide production of synthetic dyes is about  $7 \times 10^7$  tons, with over 10% of dyestuff being released as industrial wastewater [15]. Unfortunately, the discharge of nonbiodegradable dyes poses a severe threat to aquatic life and human health due to their petroleum components and lack of treatment before disposal, causing a reduction in photosynthetic activity, dissolved oxygen concentrations, and marine mortality. Traditional techniques for treating wastewater, such as biological and chemical treatments, electrochemical techniques, and physical techniques, have proven ineffective due to their high cost, low efficiency, production of toxic byproducts, secondary pollution, or the need for additional treatment. A promising method for removing these pollutants is through photocatalytic degradation using semiconductor nanoparticles. Photocatalysis is a photochemical process that accelerates a reaction's speed by converting solar energy on the surface of a semiconductor catalyst [16,17]. In this study, we utilized titanium dioxide ( $\text{TiO}_2$ ) nanoparticles, a nontoxic, cost-effective, and highly reactive photocatalyst. We used Degussa P-25  $\text{TiO}_2$ , consisting of anatase and rutile phases in a 3:1 ratio, with anatase exhibiting higher photocatalytic efficiency and rutile being more chemically stable.

Our study aims to provide insights into the potential of  $\text{TiO}_2$  nanoparticles for the photocatalytic properties of anionic dyes, specifically Amaranth, Methyl Orange, and Quinoline Yellow, commonly used in the textile industry, individually and in a multicomponent experiment. Reports in the literature showed a variable photocatalytic capacity of commercial and modified  $\text{TiO}_2$  on Amaranth, Methyl Orange, and Quinoline Yellow [18–20]. The novelty of the manuscript lies in the fact of photodegrading a mixture of dyes in an aqueous

medium (deionized water and tap water). Although a known catalyst,  $\text{TiO}_2$ , is being used, most research on photocatalysis focuses on the degradation of individual contaminants, not mixtures of them.

$\text{TiO}_2$  NPs were characterized by transmission electron microscopy (HR-TEM). The UV-Vis technique was used to track the degradation progress of the three dyes in the solution. The process was performed as a homogeneous photocatalysis, with both the  $\text{TiO}_2$  nanoparticles and the dyes in a liquid phase. The results of this study could pave the way for more efficient and eco-friendly wastewater treatment solutions.

## 2. Materials and Methods

The chemicals and raw materials were used as procured without further treatment. The P-25 Degussa  $\text{TiO}_2$  NPS (CAS 13463-67-7; F.W. 79.87 g/mol), Amaranth (CAS 915-67-3; F.W. 604.47 g/mol), Methyl Orange (CAS 547-58-0; F.W. 327.33), and Quinoline Yellow (CAS 8004-92-0; F.W. 477.38 g/mol) dyes were obtained from Sigma-Aldrich (MilliporeSigma, St. Louis, MO, USA).

The protocol for the photocatalytic degradation of Amaranth, Methyl Orange, and Quinoline Yellow, using P-25  $\text{TiO}_2$  nanoparticles, was based on our previous published work [21]. A stock solution of 500  $\mu\text{M}$  was prepared for each dye, and from this, standard solutions were derived with concentrations ranging from 3  $\mu\text{M}$ –45  $\mu\text{M}$  for AM, 1  $\mu\text{M}$ –50  $\mu\text{M}$  for MO, and 3  $\mu\text{M}$ –60  $\mu\text{M}$  for QY, to monitor their absorbances and determine the maximum wavelength. The concentrations of the P-25  $\text{TiO}_2$  nanoparticles were set at 0.010, 0.015, 0.025, and 0.050 g/L. Experimental solutions were prepared with the established concentrations of 35  $\mu\text{M}$  for AM, 30  $\mu\text{M}$  for MO, and 25  $\mu\text{M}$  for QY in an aqueous medium and tripled for each concentration, resulting in a total of eighteen solutions. Twelve of these solutions contained the dye, the established concentrations of  $\text{TiO}_2$  NPs, and deionized water, while the remaining six were used as control solutions, containing only the established concentrations of the dye and deionized water. The latter were labeled as UV and darkness blanks and were used as controls to compare the degradation progress between them and the solutions containing both the nanoparticles and dyes. For the multicomponent experiments, the same procedure was followed, but the solutions contained the concentrations of all three dyes mixed in deionized water (35  $\mu\text{M}$  for AM, 30  $\mu\text{M}$  for MO, and 25  $\mu\text{M}$  for QY). Also, an experiment of all three dyes mixed in tap water was performed.

These experimental solutions and UV blanks were subjected to photocatalytic degradation using an 8-watt UV lamp (302 nm) with power irradiation of  $10 \text{ mW}\cdot\text{cm}^{-2}$  at room temperature while being agitated in a rotamix at 20–25 rpm. The darkness blanks were placed in an unlit space under the same conditions. Samples were collected at 30 min intervals and analyzed using a UV-Vis Spectrophotometer 2700i to measure the average absorbance value and track the degradation progress of each dye. The collected samples were monitored under the maximum wavelength of absorption of each dye, which was determined to be 522 nm for AM, 464 nm for MO, and 413 nm for QY based on the absorbance spectra of the standards solutions prepared (see Supplementary Figures S2–S4). The decrease in dye concentration over time was estimated from calibration curves plotted previously (see Supplementary Figures S2–S4). Absorbance calibration curves for Amaranth, Methyl Orange, and Quinoline Yellow were plotted, covering concentrations ranging from 3  $\mu\text{M}$ –45  $\mu\text{M}$ , 1  $\mu\text{M}$ –50  $\mu\text{M}$ , and 3  $\mu\text{M}$ –60  $\mu\text{M}$ , respectively. The line equation and correlation coefficients were determined from these calibration curves.

The datasets generated and/or analyzed during the current study are available from the corresponding author upon reasonable request.

## 3. Results and Discussion

### 3.1. Morphology and Crystallography Composition of $\text{TiO}_2$

The morphological analysis at different scales depicted in Figure 1a–d offers valuable insights into the structural characteristics of  $\text{TiO}_2$  nanoparticles (surface area 35–65  $\text{m}^2/\text{g}$ , BET, band gap of 3.20 eV), which are essential for understanding their behavior in various

applications such as photocatalysis. The spherical shape and tendency to aggregate observed in the nanoparticles (average size of 21 nm) are consistent with previous research findings, highlighting the importance of surface energy minimization in nanoparticle systems. The presence of faceted features and chain configurations among the particles suggests potential crystalline facets and directional growth, indicating the complexity of TiO<sub>2</sub> nanoparticle assembly. Furthermore, the coexistence of amorphous particles alongside crystalline phases (anatase and rutile) adds depth to the understanding of the nanoparticle system's composition. Energy-dispersive X-ray studies offer insights into the elemental composition of TiO<sub>2</sub> NPs. Analysis of TiO<sub>2</sub> samples revealed a composition (expressed in atomic percentage) of 33% titanium and 67% oxygen (spectrum is not shown here), unequivocally confirming the predominance of Ti and O as the primary constituents of these nanostructures. In addition to confirming the predominant presence of titanium and oxygen in TiO<sub>2</sub> NPs, the EDX analysis confirmed the absence of any impurities or dopants within the nanostructures.

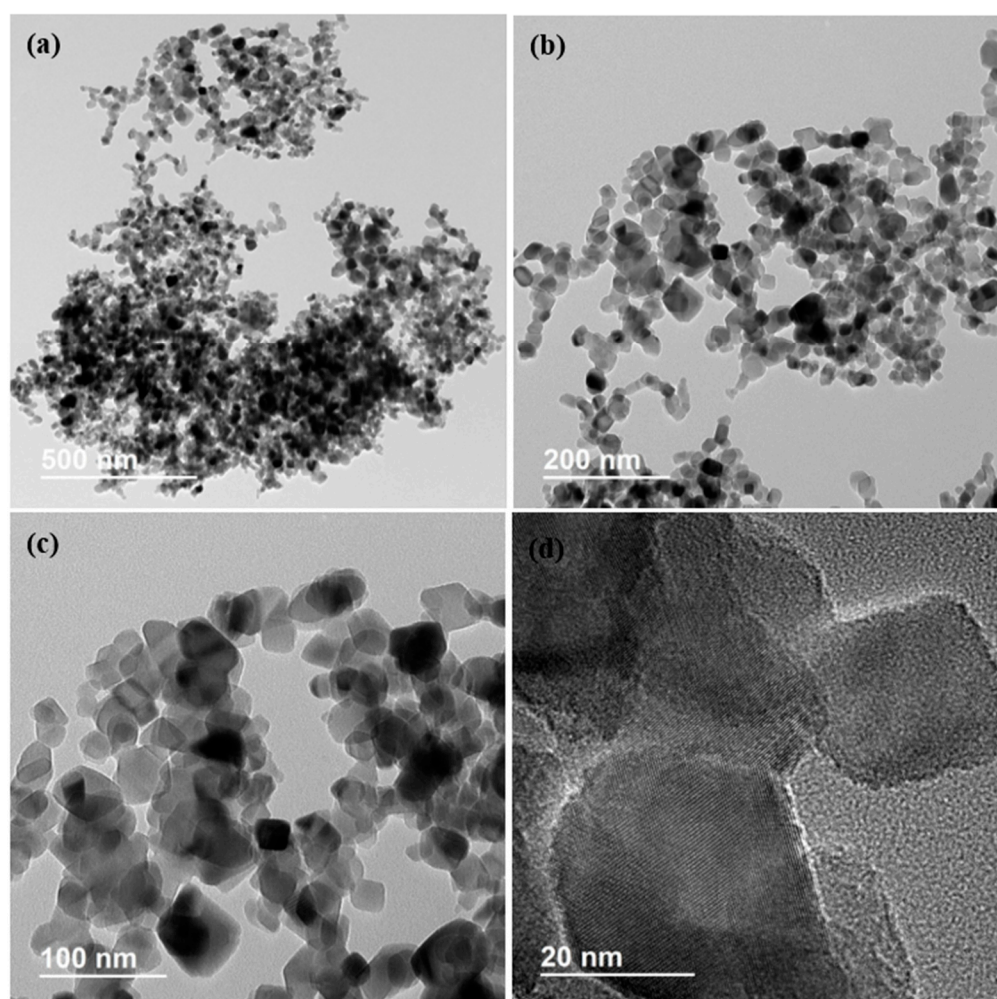


**Figure 1.** (a–c) Low-magnification TEM images of TiO<sub>2</sub> NPs, and (d) HR-TEM image of TiO<sub>2</sub> nanoparticles.

### 3.2. Photocatalytic Degradation of AM, MO, and QY

The study explores the catalytic potential of titanium dioxide nanoparticles in the photodegradation process of organic dyes. To comprehensively assess their efficacy, three distinct dyes: Amaranth, Methyl Orange, and Quinoline Yellow, were subjected to experimentation. Varied concentrations of TiO<sub>2</sub> (0.010, 0.015, 0.025, and 0.050 g/L) were employed under UV irradiation conditions. Throughout the experiment, the relative concentrations of the dyes ( $C_f/C_i$ ) were monitored and recorded (Figures 2–4). The findings provide

compelling evidence that the photodegradation process is intricately linked to both the concentration of TiO<sub>2</sub> nanoparticles and the duration of UV irradiation. Control groups subjected to UV light exposure in the presence of dye and those kept in darkness while in contact with the dyes (for Amaranth, Methyl Orange, and Quinoline Yellow) exhibited minimal degradation throughout the experiment. This observation strongly suggests that the observed decrease in dye concentration can be primarily attributed to the degradation catalyzed by the TiO<sub>2</sub> nanoparticles.

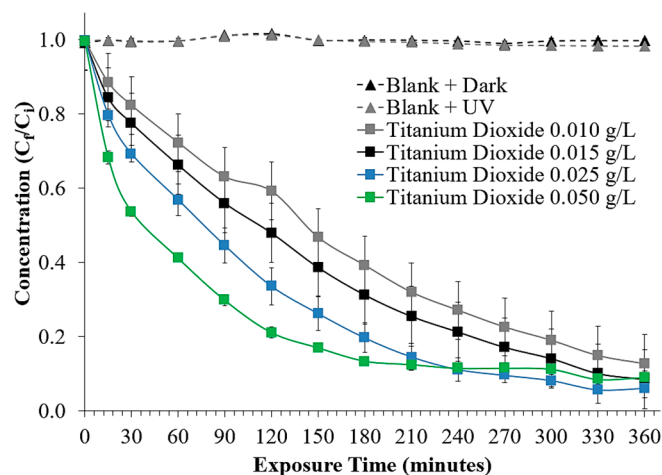


**Figure 2.** Photocatalytic activity of TiO<sub>2</sub> NPs at 4 concentrations (0.010, 0.015, 0.025, and 0.050 g/L) for the degradation of Amaranth.

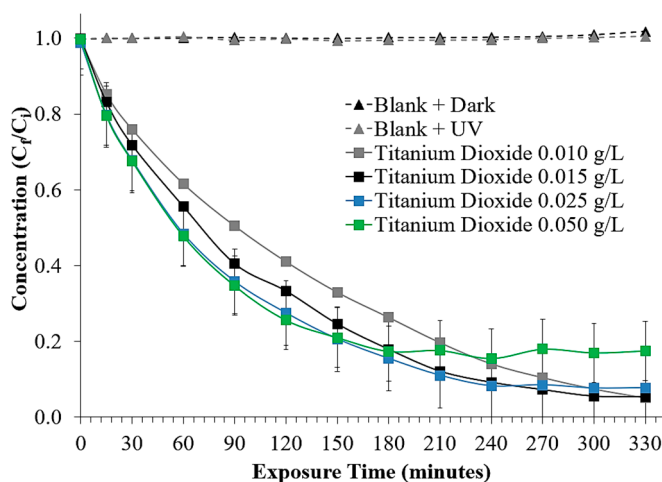


**Figure 3.** Photocatalytic activity of TiO<sub>2</sub> NPs at four concentrations (0.010, 0.015, 0.025, and 0.050 g/L) for the degradation of Methyl Orange.

For Amaranth, the degradation efficiency varied with the concentration of TiO<sub>2</sub> nanoparticles. Specifically, the 0.025 g/L TiO<sub>2</sub> nanoparticles exhibited the highest efficacy, degrading 94% of the dye within 360 min of irradiation. Meanwhile, concentrations of 0.010, 0.015, and 0.050 g/L resulted in slightly lower degradation percentages of 87%, 92%, and 91%, respectively (Figure 2). In the case of Methyl Orange, optimal degradation occurred with 0.015 g/L TiO<sub>2</sub> nanoparticles, which effectively decomposed 97% of the dye after 330 min of irradiation. Contrarily, lower and higher concentrations (0.010, 0.025, and 0.050 g/L) displayed slightly lower degradation rates of 81%, 93%, and 82%, respectively (Figure 3). Interestingly, for Quinoline Yellow, the trend differed. The 0.010 and 0.015 g/L TiO<sub>2</sub> nanoparticles demonstrated remarkable efficiency, degrading 99% of the dye after 360 min of irradiation, surpassing the performance of higher concentrations. In contrast, the 0.025 and 0.050 g/L TiO<sub>2</sub> nanoparticles exhibited slightly lower degradation rates of

88% and 77%, respectively (Figure 4). This trend suggests that for all three dyes, the degradation efficiency peaks at lower concentrations of TiO<sub>2</sub> nanoparticles, indicating a nuanced relationship between nanoparticle concentration and dye degradation effectiveness.

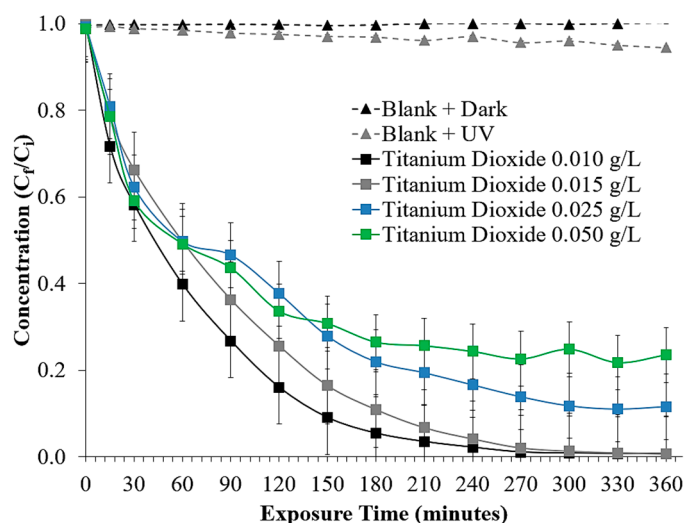


**Figure 4.** Photocatalytic activity of TiO<sub>2</sub> NPs at four concentrations (0.010, 0.015, 0.025, and 0.050 g/L) for the degradation of Quinoline Yellow.

The catalyst concentration plays an important role in the photocatalytic capacity of TiO<sub>2</sub> nanoparticles. Increasing the catalyst concentration promotes greater generation of ROS initially, resulting in enhanced dye photodegradation. However, the concentration of the catalyst is not the only parameter that affects the photocatalysis processes. In Figures 2–4, it is evident that in the early stages, TiO<sub>2</sub> at high concentration (0.050 g/L) promotes fast degradation. However, after the reaction is stopped and in the final stages of the degradation process, lower concentrations of TiO<sub>2</sub> demonstrate greater efficiency. Since the light intensity, illumination time, and concentrations of oxygen, among other parameters, remain constant during the entire process, this leads to decreased efficiency of photodegradation at higher catalyst concentrations (0.050 g/L of TiO<sub>2</sub>). It is known that the generation of ROS depends on the oxygen concentration in the solution. Higher concentrations of oxygen and catalyst will promote more generation of ROS. In this case, the concentration of oxygen was constant for all TiO<sub>2</sub> concentrations, which did not promote a high production of ROS at high concentrations of TiO<sub>2</sub> [22].

In TiO<sub>2</sub>, the valence band is primarily formed by the bonding orbitals of oxygen and titanium. Oxygen's 2p orbitals hybridize with titanium's 3d orbitals to form the valence band, indicating a significant contribution from both elements to the electronic structure. This hybridization influences the material's electronic properties and its ability to participate in redox reactions during photocatalysis. On the other hand, the conduction band consists mainly of titanium's 3d orbitals. This indicates that electrons in the conduction band are primarily associated with titanium atoms, suggesting that titanium plays a dominant role in charge transport within the material. During UV-based advanced oxidation processes (AOPs), such as photocatalysis, TiO<sub>2</sub> nanomaterials were irradiated with photons of energy greater than 3.2 electron volts (eV); in this study, with UV light at 302 nm. These photons have sufficient energy to excite electrons from the valence band to the conduction band, creating electron–hole pairs (photoinduced charge carriers). The excited electron in the conduction band becomes mobile and can participate in reduction reactions, while the hole left behind in the valence band can engage in oxidation reactions [23,24].

The photodegradation process hinges on the transformative interplay of UV-activated TiO<sub>2</sub> nanoparticles with organic contaminants. The generated photoinduced charge carriers are highly reactive and subsequently migrate to the surface of the nanoparticles. Here, they engage in redox reactions with adsorbed water molecules or oxygen, producing reactive

oxygen species (ROS) such as hydroxyl radicals ( $\bullet\text{OH}$ ) and superoxide radicals ( $\bullet\text{O}_2^-$ ). The generated ROS are potent oxidizing agents capable of abstracting hydrogen atoms from organic molecules or directly attacking carbon–carbon double bonds, leading to the fragmentation and eventual mineralization of the contaminant into smaller, less harmful molecules. This cascade of oxidation reactions effectively dismantles complex organic pollutants, rendering them less persistent and more amenable to further degradation or complete mineralization into harmless byproducts such as carbon dioxide and water. Furthermore, the unique surface properties of  $\text{TiO}_2$  nanoparticles, including their expansive surface area and the presence of surface defects, play a pivotal role in augmenting the efficiency of the photodegradation process. These attributes facilitate the adsorption of organic contaminants onto the nanoparticle surface, thereby enhancing the probability of interaction with photoexcited charge carriers and fostering degradation reactions [25,26].

Overall, the photodegradation mechanism mediated by  $\text{TiO}_2$  nanoparticles underscores their potential as promising catalysts for the remediation of environmental pollutants, offering a sustainable and environmentally benign approach to wastewater treatment and pollution mitigation.

### 3.3. Photocatalytic Degradation of the Multicomponent

As discussed previously in Figures 2–4, titanium dioxide nanoparticles were efficient in the individual photodegradation of Amaranth, Methyl Orange, and Quinoline Yellow. However, dyes may be discharged into water bodies in the form of mixtures. Therefore, the photodegradation capacity of titanium dioxide was evaluated in complex systems, specifically, on a mixture of Amaranth, Methyl Orange, and Quinoline Yellow in deionized water.

Figure 5a–c show the photodegradation curves for Amaranth, Methyl Orange, and Quinoline Yellow in the multicomponent after 330 min of irradiation. In the case of AM, the 0.050 g/L  $\text{TiO}_2$  degraded 40% of the dye, whereas the 0.010, 0.015, and 0.025 g/L  $\text{TiO}_2$  degraded 17%, 22%, and 31% of the dye, respectively. For MO, the 0.050 g/L  $\text{TiO}_2$  degraded 39% of the dye, while the 0.010, 0.015, and 0.025 g/L  $\text{TiO}_2$  degraded 16%, 22%, and 30% of the dye, respectively. Regarding QY, the 0.050 g/L  $\text{TiO}_2$  degraded 38% of the dye, while the 0.010, 0.015, and 0.025 g/L  $\text{TiO}_2$  degraded 15%, 20%, and 29% of the dye, respectively. In each case, despite the 0.050 g/L  $\text{TiO}_2$  degrading a higher percentage of the multicomponent, the other concentrations of nanoparticles demonstrated noteworthy degradation of the three dyes in the mixture. This underscores the robustness of the photodegradation process mediated by  $\text{TiO}_2$  nanoparticles, wherein even lower concentrations exhibit considerable efficacy in degrading multiple dyes simultaneously.

The photodegradation mechanism of the studied anionic dyes may be due to the initial destruction of the nitrogen–nitrogen double bond responsible for the color in the Amaranth and Methyl Orange dyes. The presence of light-activated  $\text{TiO}_2$  is expected to generate electron–hole pairs, followed by reactive oxygen species (ROS) formation. These ROS would be responsible for breaking the nitrogen double bond in the anionic dye molecules. Furthermore, the degradation of Quinoline Yellow could occur primarily through the attack of the pyridine ring (lower electron density in comparison to benzene rings) by the superoxide radicals (a type of ROS).

It is important to highlight that, similar to Figures 2–4 (individual dyes), the photodegradation of the dye mixture, as evidenced in Figure 5, indicates that  $\text{TiO}_2$  at higher concentrations exhibits significant photodegradation efficiency in the early stages of the process compared to other concentrations used. However, it is later observed that photodegradation stops and remains constant until 360 min. As explained previously, the catalyst concentration is not the only factor governing photocatalysis. There are other factors involved in the process, such as the intensity of illumination, duration of irradiation intervals, and oxygen concentration, among others.

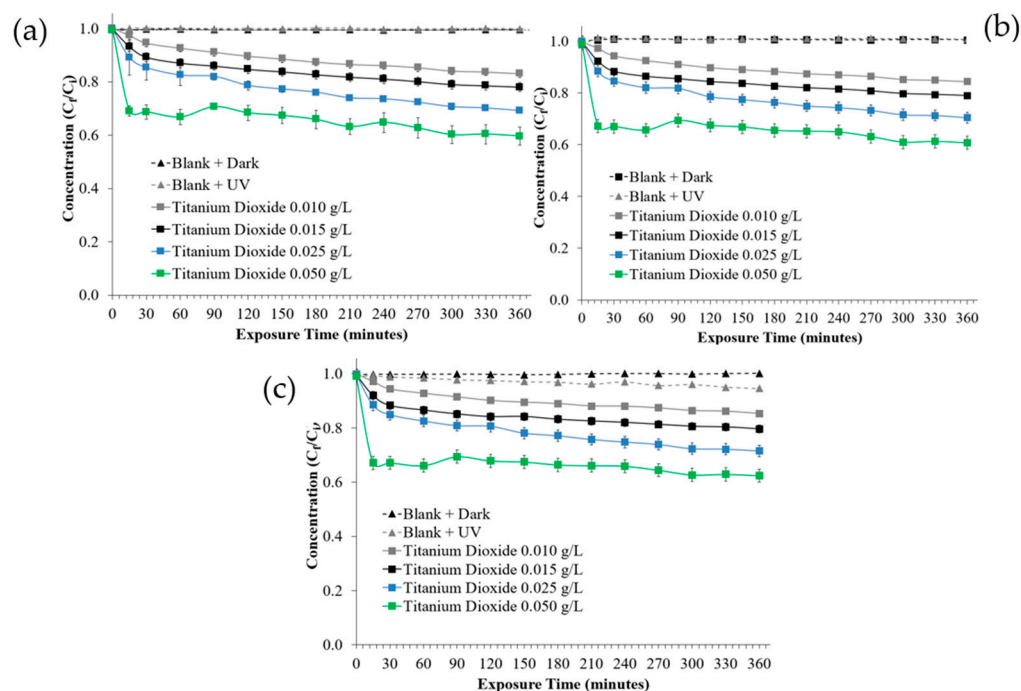


**Figure 5.** Photocatalytic activity of TiO<sub>2</sub> NPs at four concentrations (0.010, 0.015, 0.025, and 0.050 g/L) for the degradation of (a) Amaranth, (b) Methyl Orange, and (c) Quinoline Yellow in the multicomponent experiments.

In this research, we conducted a multicomponent test using tap water instead of deionized water. The tap water utilized in the experiments was sourced directly from the University of Puerto Rico in Ponce, drawn from the water supply used within the chemistry laboratories. This decision was motivated by the need to simulate real-world conditions more accurately and assess how the presence of minerals and other impurities commonly found in tap water might influence the photocatalytic activity of nanoparticles. Understanding the behavior of nanoparticles in such complex environmental matrices is crucial for extrapolating laboratory findings to practical applications, particularly in wastewater treatment scenarios. Figure 6 displays the photodegradation curves for Amaranth, Methyl Orange, and Quinoline Yellow after 330 min of light exposure.

For AM, the use of 0.050 g/L TiO<sub>2</sub> resulted in a 52% degradation of the dye, whereas 0.010, 0.015, and 0.025 g/L TiO<sub>2</sub> degraded 10%, 13%, and 27%, respectively. Similarly, for MO, 0.050 g/L TiO<sub>2</sub> achieved a degradation of 50%, while the concentrations of 0.010, 0.015, and 0.025 g/L degraded 12%, 15%, and 27%, respectively. In the case of QY, 0.050 g/L TiO<sub>2</sub> degraded 49%, while 0.010, 0.015, and 0.025 g/L degraded 11%, 14%, and 26%, respectively. Notably, the 0.050 g/L TiO<sub>2</sub> consistently achieved around 50% degradation across all three dyes, a significantly higher percentage compared to our previous multicomponent experiment. The notable improvement in dye degradation observed when using tap water as opposed to deionized water prompts a deeper examination of the factors at play. Tap water, sourced from natural environments, typically contains a diverse array of minerals and organic compounds, which can act as co-catalysts or promoters in photocatalytic processes. These minerals, such as calcium, magnesium, and bicarbonates, may interact synergistically with TiO<sub>2</sub> nanoparticles, facilitating electron transfer processes and enhancing the generation of reactive oxygen species (ROS) under UV irradiation.

Furthermore, the presence of natural organic matter (NOM) in tap water can serve as additional electron donors, further promoting the photocatalytic activity of TiO<sub>2</sub> nanoparticles. NOM contains a variety of functional groups, such as carboxyl, hydroxyl, and phenolic groups, which can scavenge photogenerated holes, thereby inhibiting charge recombination and prolonging the lifetime of photoinduced charge carriers. This prolonged availability of active charge carriers enhances the efficiency of dye degradation reactions.

Additionally, tap water may also contain trace amounts of metal ions, such as iron and copper, which can act as Fenton-like catalysts, generating additional ROS through the Haber–Weiss reaction. These ROS can then participate in secondary oxidation reactions, leading to further degradation of the dye molecules [27,28].

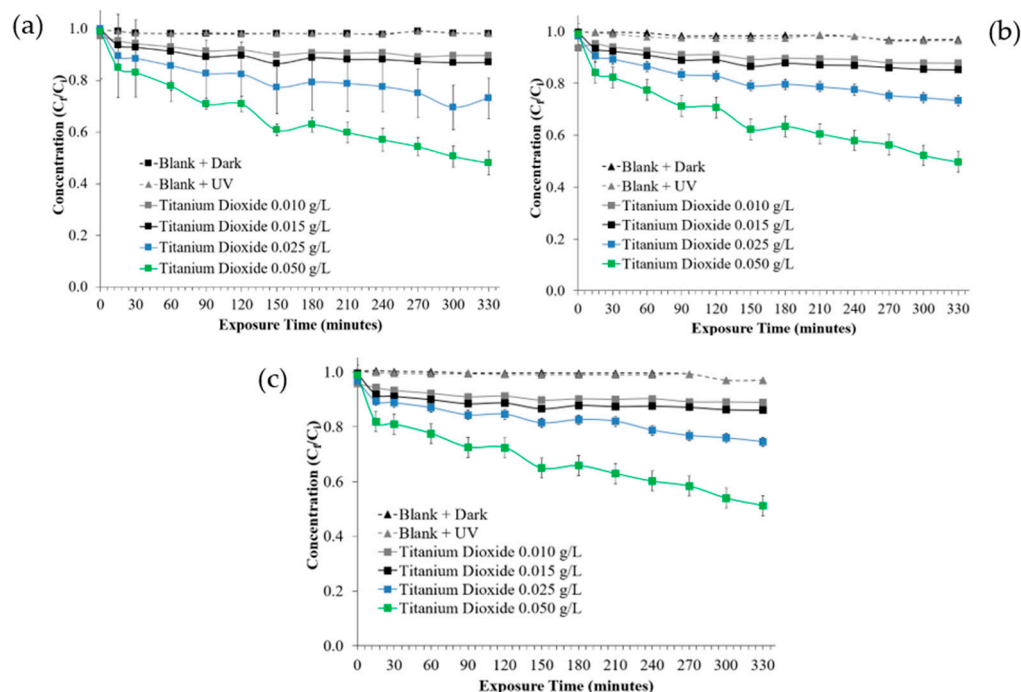


**Figure 6.** Photocatalytic activity of  $\text{TiO}_2$  NPs at four concentrations (0.010, 0.015, 0.025, and 0.050 g/L) for the degradation of (a) Amaranth, (b) Methyl Orange, and (c) Quinoline Yellow in the multicomponent experiments using tap water.

In summary, the enhanced photodegradation observed in tap water can be attributed to the complex interplay of minerals, organic matter, and metal ions present in the water matrix, which synergistically promote the photocatalytic activity of  $\text{TiO}_2$  nanoparticles. This underscores the importance of considering the composition of the water matrix when evaluating the performance of photocatalytic processes in real-world applications.

#### 4. Conclusions

This study explores the breakdown of anionic dyes Amaranth, Methyl Orange, and Quinoline Yellow through photocatalysis using titanium dioxide nanoparticles. The results indicate that, for Amaranth, a concentration of 0.025 g/L of nanoparticles demonstrated superior efficiency, achieving a 94% degradation in 360 min, outperforming concentrations of 0.010, 0.015, and 0.050 g/L. In the case of Methyl Orange, the most effective concentration was 0.015 g/L, achieving a remarkable 97% degradation after 330 min of irradiation. Similarly, for Quinoline Yellow, concentrations of 0.010 and 0.015 g/L proved more efficient, achieving a 99% degradation after 330 min of irradiation. Two multicomponent experiments were conducted by mixing the three dyes in a solution, one with deionized water and the other with tap water. After 330 min of irradiation, the 0.050 g/L concentration showed enhanced efficiency, degrading approximately 40% and 50% of the three dyes in the deionized and tap water solutions, respectively. The results suggest that minerals in tap water could play a role in promoting the titanium dioxide nanoparticles' effectiveness in degrading these dyes.

**Supplementary Materials:** The following supporting information can be downloaded at: <https://www.mdpi.com/article/10.3390/photochem4020014/s1>, Figure S1: Skeletal structures of (a) Amaranth, (b) Methyl Orange, and (c) Quinoline Yellow, all anionic dyes. Figure S2: (a) UV–Vis spectra and (b) calibration curve of Amaranth. Figure S3: (a) UV–Vis spectra and (b) calibration curve of Methyl Orange. Figure S4: (a) UV–Vis spectra and (b) calibration curve of Quinoline Yellow.

**Author Contributions:** Conceptualization, S.J.B.-R. and A.A.L.-R.; funding acquisition, S.J.B.-R.; methodology, S.J.B.-R. and A.A.L.-R.; writing—original draft, S.J.B.-R. and A.A.L.-R.; writing—review and editing, S.J.B.-R. and A.A.L.-R. All authors have read and agreed to the published version of the manuscript.

**Funding:** This research was supported by institutional funds of the University of Puerto Rico at Ponce, the National Science Foundation under Grant No. 2313252, the Department of Defense/US Army No. W911NF-21-1-0206, and the Beta Beta Beta Research Scholarship Foundation.

**Data Availability Statement:** Data are contained within the article and Supplementary Materials.

**Acknowledgments:** The research was conducted at the Laboratory of Investigation in Nanotechnology and Characterization (LINC). We thank the support of the Department of Chemistry and Physics at the UPRP, and the National High Magnetic Field Laboratory supported by the National Science Foundation Cooperative Agreement No. DMR-2128556 and the State of Florida.

**Conflicts of Interest:** The authors declare no conflicts of interest. The funders had no role in the design of the study; in the collection, analyses, or interpretation of data; in the writing of the manuscript; or in the decision to publish the results.

## References

1. Yadav, S.; Tiwari, K.S.; Gupta, C.; Tiwari, M.K.; Khan, A.; Sonkar, S.P. A brief review on natural dyes, pigments: Recent advances and future perspectives. *Results Chem.* **2023**, *5*, 100733. [CrossRef]
2. Benkhaya, S.; Rabet, S.M.; Harfi, A.E. A review on classifications, recent synthesis and applications of textile dyes. *Inorg. Chem. Commun.* **2020**, *115*, 107891. [CrossRef]
3. IARC Working Group on the Evaluation of Carcinogenic Risks to Humans. Some Aromatic Amines, Organic Dyes, and Related Exposures. Lyon (FR): International Agency for Research on Cancer. 2010; (IARC Monographs on the Evaluation of Carcinogenic Risks to Humans, No. 99). General Introduction to the Chemistry of Dyes. Available online: <https://www.ncbi.nlm.nih.gov/books/NBK385442> (accessed on 10 December 2023).
4. Kagathara, M.; Dalal, D.J.; Solanki, H.A. Revealing Explanation on Organic Dyes: A Review. *Int. J. Res. Advent Technol.* **2020**, *8*, 1–8. [CrossRef]
5. Slama, H.B.; Chenari Bouket, A.; Pourhassan, Z.; Alenezi, F.N.; Silini, A.; Cherif-Silini, H.; Oszako, T.; Luptakova, L.; Golińska, P.; Belbahri, L. Diversity of Synthetic Dyes from Textile Industries, Discharge Impacts and Treatment Methods. *Appl. Sci.* **2021**, *11*, 6255. [CrossRef]
6. Affat, S. Classifications, Advantages, Disadvantages, Toxicity Effects of Natural and Synthetic Dyes: A review. *UTJsci.* **2021**, *8*, 130–135.
7. Fobiri, G.K. Synthetic Dye Application in Textiles: A Review on the Efficacies and Toxicities Involved. *Text. Leather Rev.* **2022**, *5*, 180–198. [CrossRef]
8. Islam, M.T.; Islam, T.; Islam, T.; Repon, M.R. Synthetic Dyes for Textile Colouration: Process, Factors and Environmental Impact. *Text. Leather Rev.* **2022**, *5*, 327–373. [CrossRef]
9. Amaranth Dye Content 85-95 915-67-3. Available online: <https://www.sigmaaldrich.com/US/en/product/sigma/a1016> (accessed on 23 February 2024).
10. PubChem. Amaranth. Available online: <https://pubchem.ncbi.nlm.nih.gov/compound/Amaranth> (accessed on 23 February 2024).
11. Methyl Orange ACS Reagent, Dye Content 85 547-58-0. Available online: <https://www.sigmaaldrich.com/US/en/product/sial/114510> (accessed on 23 February 2024).
12. PubChem. Methyl Orange. Available online: <https://pubchem.ncbi.nlm.nih.gov/compound/Methyl-orange> (accessed on 23 February 2024).
13. Quinoline Yellow Mixture of the Mono- and Disulfonic Acids of Quinoline Yellow 8004-92-0. Available online: <https://www.sigmaaldrich.com/US/en/product/sial/309052> (accessed on 23 February 2024).
14. PubChem. Acid Yellow 3. Available online: <https://pubchem.ncbi.nlm.nih.gov/compound/Acid-yellow-3> (accessed on 23 February 2024).
15. Chandanshive, V.V.; Kadam, S.K.; Rane, N.R.; Jeon, B.; Jadhav, J.P.; Govindwar, S.P. In situ textile wastewater treatment in high-rate transpiration system furrows planted with aquatic macrophytes and floating phytobeds. *Chemosphere* **2020**, *252*, 126513. [CrossRef]

16. Al-Tohamy, R.; Ali, S.S.; Li, F.; Okasha, K.; Mahmoud, Y.A.; Elsamahy, T.; Jiao, H.; Fu, Y.; Sun, J. A critical review on the treatment of dye-containing wastewater: Ecotoxicological and health concerns of textile dyes and possible remediation approaches for environmental safety. *Ecotoxicol. Environ. Saf.* **2022**, *231*, 113160. [[CrossRef](#)]
17. Ajmal, A.; Majeed, I.; Malik, R.N.; Idriss, H.; Nadeem, M.A. Principles and mechanisms of photocatalytic dye degradation on TiO<sub>2</sub> based photocatalysts: A comparative overview. *RSC Adv.* **2014**, *4*, 37003–37026. [[CrossRef](#)]
18. Moncada-Sánchez, C.; Salazar-Hernández, M.; Baltazar-Vera, J.C.; Caudillo-González, M. Degradation of AMARANTH with TiO<sub>2</sub> Synthesized by Sol-Gel Process. *ECOREFAN J. Bolív.* **2022**, *9*, 9–14. [[CrossRef](#)]
19. Razali, M.H.; Dris, M.M.; Rudin, N.M. Photodegradation of methyl orange dye using titanium dioxide photocatalyst. *J. Sustain. Sci. Manag.* **2009**, *4*, 49–55.
20. Gupta, D.; Chauhan, R.; Kumar, N.; Singh, V.; Srivastava, V.C.; Mohanty, P.; Mandal, T.K. Enhancing photocatalytic degradation of quinoline by ZnO: TiO<sub>2</sub> mixed oxide: Optimization of operating parameters and mechanistic study. *J. Environ. Manag.* **2020**, *258*, 110032. [[CrossRef](#)] [[PubMed](#)]
21. Lugo-Ruiz, A.A.; Paz-Ruiz, M.J.; Bailón-Ruiz, S.J. Degradation of organic dyes in the presence of titanium-based nanoparticles. *MRS Adv.* **2022**, *7*, 289–294. [[CrossRef](#)]
22. Nawawi, W.I.; Zaharudin, R.; Zuliahani, A.; Shukri, D.S.; Azis, T.F.; Razali, Z. Immobilized TiO<sub>2</sub>-Polyethylene Glycol: Effects of Aeration and pH of Methylene Blue Dye. *Appl. Sci.* **2017**, *7*, 508. [[CrossRef](#)]
23. Ćurković, L.; Ljubas, D.; Šegota, S.; Bačić, I. Photocatalytic degradation of Lissamine Green B dye by using nanostructured sol-gel TiO<sub>2</sub> films. *J. Alloys Compd.* **2014**, *604*, 309–316. [[CrossRef](#)]
24. Ngoh, Y.S.; Nawi, M.A. Fabrication and properties of an immobilized P25 TiO<sub>2</sub>-montmorillonite bilayer system for the synergistic photocatalytic-adsorption removal of methylene blue. *Mater. Res. Bull.* **2016**, *76*, 8–21. [[CrossRef](#)]
25. Ljubas, D.; Juretić, H.; Badrov, A.; Biošić, M.; Babić, S. Photocatalytic Degradation of Pharmaceutical Trimethoprim in Aqueous Solution over Nanostructured TiO<sub>2</sub> Film Irradiated with Simulated Solar Radiation. *Appl. Sci.* **2023**, *13*, 5681. [[CrossRef](#)]
26. Krakowiak, R.; Musiał, J.; Bakun, P.; Spychała, M.; Czarczynska-Goslinska, B.; Mlynarczyk, D.T.; Koczorowski, T.; Sobotta, L.; Stanisz, B.; Goslinski, T. Titanium Dioxide-Based Photocatalysts for Degradation of Emerging Contaminants including Pharmaceutical Pollutants. *Appl. Sci.* **2021**, *11*, 8674. [[CrossRef](#)]
27. Fattahi, A.; Jaciw-Zurakowsky, I.; Srikanthan, N.; Bragg, L.; Liang, R.; Zhou, N.; Servos, M.; Arlos, M. Effect of Background Water Matrices on Pharmaceutical and Personal Care Product Removal by UV-LED/TiO<sub>2</sub>. *Catalysts* **2021**, *11*, 576. [[CrossRef](#)]
28. Ahmad, S.; Almeahadi, M.; Janjuhah, H.T.; Kontakiotis, G.; Abdulaziz, O.; Saeed, K.; Ahmad, H.; Allahyani, M.; Aljuaid, A.; Alsaiani, A.A.; et al. The Effect of Mineral Ions Present in Tap Water on Photodegradation of Organic Pollutants: Future Perspectives. *Water* **2023**, *15*, 175. [[CrossRef](#)]

**Disclaimer/Publisher’s Note:** The statements, opinions and data contained in all publications are solely those of the individual author(s) and contributor(s) and not of MDPI and/or the editor(s). MDPI and/or the editor(s) disclaim responsibility for any injury to people or property resulting from any ideas, methods, instructions or products referred to in the content.